

Fluid Dynamic Efficiency Optimization of Steam Turbine Stages Considering Leakage Influences and Inter-stage Reciprocal Interferences

Xin Yuan¹, Qian Pu¹, Xiaofeng Zhu¹, Zhirong Lin¹, Yoshiki Niizeki², Naoki Shibukawa² and Tadashi Tanuma³

¹ Department of Thermal Engineering, Tsinghua University
Beijing 100084, P.R. CHINA

² Toshiba Corporation, JAPAN

³ Teikyo University, JAPAN

ABSTRACT

An optimization method for three-dimensional turbine blade design including end wall contouring control with non-axis-symmetric geometry has been developed. This design optimization method consists of three-dimensional parametric modeling module for blades and end walls, optimization algorithm module and the design evaluation method using Computational Fluid Dynamics code.

This paper presents the advanced and more applicative study to enhance this optimization methodology from a single turbine stage to two turbine stages with stator blade hub leakage and rotor blade tip leakage influences.

Results of present fluid dynamic design optimization study with consideration of tip and hub leakage show that the efficiency of the current well designed high pressure steam turbine stage has been enhanced by 0.21%. Using parallel optimization algorithm and a cluster PC system, the design cycle can be shortened to seven days for an optimization with one thousand iterations of two turbine stage CFD on 20 CPUs of 2.0G cluster PC.

NOMENCLATURE

$A(u)$	The position of a point on the curve
h_{0T}	First stage inlet total enthalpy
h_{2s}	Second stage outlet isentropic enthalpy
\dot{m}	Mass flow rate
$N_{i,p}(u)$	B-spline basis functions
<i>NURBS</i>	Non-Uniform Rational B Spline
P_i	Control points coordinates
u	Parameter of NURBS curve
$\Delta R(s, t)$	Radial coordinate change function, where s and t are normalized axial and circumferential coordinates respectively.
Greek	
η	Total to static enthalpy efficiency of two stages
ω_i	Respective weights

INTRODUCTION

Large-scale steam turbines are part of the core machinery for fossil and nuclear electric power generation plants. Accordingly,

customers' requirements to enhance the efficiency of steam turbines are getting larger aiming to decrease their emission of carbon dioxide gas from fossil power plants and to increase electrical power output from their nuclear power plants. An optimization method for three-dimensional turbine blade design including its end wall contouring control with non-axis-symmetric geometry has been developed. This design optimization method consists of three-dimensional parametric modeling module for blades and end walls, optimization algorithm module and the design evaluation method using Computational Fluid Dynamics codes. For the blade three-dimensional modeling, a Non-Uniform Rational B-Spline (NURBS) technology is chosen for two-dimensional (2D) blade profile parameterization. The 3D blade surface is constructed by NURBS skinning technology. The Design of Experiments (DOE) method is employed to explore the high-dimensional design space and choose most influential parameters as design variables. The Genetic Algorithm (GA) is applied for global exploration. The Response Surface Method (RSM) for approximation is constructed by fitting the results from the DOE and GA processes. RSM is optimized using the Sequential Quadratic Programming (SQP) for local refinement. A typical high pressure steam turbine stage of stator blades and rotating blades with rotor tip leakage for large-scale steam turbines were optimized successfully using the developed system in previous study. [1].

Meanwhile the labyrinth seal leakage flow has been considered as an inevitable factor that highly affects the efficiency of shrouded steam turbine stages. Researches on seal leakage flows in turbine stages can be traced back to the 1960s, which were carried out mainly experimentally and theoretically. As the requirements of efficiency improvements become larger and the numerical research methods become more advanced, labyrinth seal leakage has received wide attention recently. Wallis et al. [2] studied a single fin seal structure on the tip of a high pressure turbine stage by experiments and numerical simulations, expecting to reduce leakage mass flow rate and to reduce the loss caused by the leaving and re-injection of leakage flows. Porreca et al. [3] made a comparative experimental and numerical investigation on two test cases of shroud configurations, with different labyrinth seal paths. Rosic et al. [4] carried out three kinds of three-dimensional steady multi-stage calculations and compared the results with experimental measurement in a low-speed three-stage model turbine. Pfau et al. [5] examined the flow interactions set up by the presence of labyrinth seals using the control volume analysis and the radial equilibrium of forces acting on streamlines and derived design recommendations. Rosic et al. [6] carried out some three-dimensional multi-block calculations in the model of a 1.5 stage turbine. By varying the shroud geometry systematically and testing the varied cases numerically, they investigated the influence of geometric

modifications on mainstream aerodynamics and obtained a map of the possible turbine efficiency changes caused by different shroud geometries. All these works have emphasized the importance of the study of labyrinth seal leakage in low aspect ratio steam turbines and the necessity of considering leakage flows in turbine blade designs.

This paper presents the advanced and more applicative study to enhance the developed optimization methodology of our research group from a single turbine stage to two turbine stages with stator blade hub leakage and rotor blade tip leakage influences. In this two stage optimum design study, a package CFD code with a leakage flow modeling using our design empirical equation of leakage mass flow rate was used for the design evaluation module in the optimization system in order to enhance the evaluation accuracy considering leakage influences within the acceptable CPU time. Multi-objective optimization, named NSGA-II (non-dominated sorting genetic algorithms) optimization strategy was used in the optimum design module for the current two stage design optimization. Typical two successive stages for large scale steam turbines with hub leakage in stator blades and tip leakage in rotating blades were optimized using the present developed system. The detail results of two successive stage optimization considering leakage influences and inter-stage reciprocal interferences are presented in this paper.

AERODYNAMIC OPTIMIZATION SYSTEM

The present optimization system is developed to assist turbine designers to coordinate their knowledge of aerodynamics with modern optimization technologies, to expand design exploration scopes and to accelerate design processes of high efficiency steam turbine stages with stator and rotor blades. The optimization system is integrated as shown in Figure 1, where the commercial package components are marked by a star mark (*).

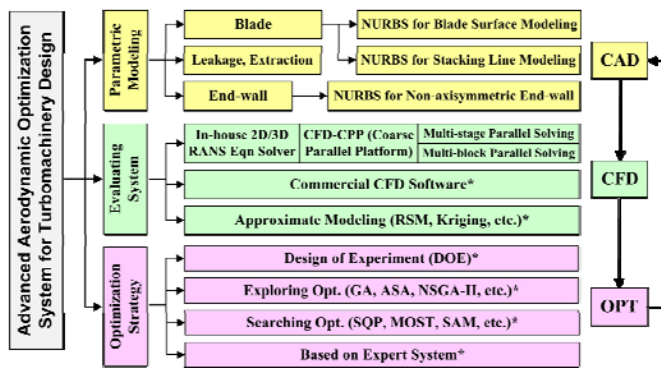


Fig. 1 Aerodynamic optimization design system

There are three modules in the optimization design system. The first is the Parametric Modelling System, in which the Non-Uniform Rational B-Spline (NURBS) is used for three-dimensional geometric representations for blades and end-walls. The second is the Evaluating System, where either the in-house higher-order Reynolds-Averaged Navier-Stokes (RANS) equation code with the ability to analysis real steam flows [7-9] or commercial Navier-Stokes CFD solvers can be used to evaluate the performance of the turbine stages. In the Approximate Modelling component of Evaluating System, besides using the knowledge gained during previous designs, other software modules like the Response Surface Method (RSM) and Kriging Interpolation Method can also be used to approximate the performance of new blades. The third module is the Optimization Strategy System, where a computer aided optimization package software is applied.

Blade Three-Dimensional Geometric Representation

The parametrical modelling of blade geometries is of great importance in the optimization process. Effective design param-

eters must be chosen and suitable limitations must be set for these parameters as to reduce the number of design variables and still remain high design flexibilities. NURBS technology is an ideal way to achieve this goal.

In the present optimization system, a blade is modelled in the form of control sections and its blade stacking line. Blade control sections are represented by NURBS composite curves, and this parameterization is achieved by using the Sequential Quadratic Programming (SQP) to solve an inverse analysis for the control points and minimize the error in the representation. The blade stacking line is also represented by NURBS curves since the NURBS curves are highly flexible in blade deformations as lean, sweep and twist, and in the meantime could remain remarkable accuracy. After that, NURBS skinning technology is applied to reconstruct blades with their 2D blade control profiles and the stacking line [10].

A NURBS curve is given by a weighted average of all control points P_i . The weight function is a B-spline basis function

$N_{i,p}(u)$ times a weight ω_i . Therefore, once the control points and the corresponding weights are specified, the blade profile or the blade stacking line is determined. A NURBS curve is defined as follows [11],

$$A(u) = \frac{\sum_{i=0}^n W_{i,p}(u) P_i}{\sum_{i=0}^n W_{i,p}(u)} \quad (1)$$

where

$$W_{i,p} = N_{i,p}(u) \omega_i \quad (2)$$

In which P_i represent control points coordinates, ω_i their respective weights, $N_{i,p}(u)$ the pth-degree B-Spline basis functions and $A(u)$ the position of a point on the curve [11]. The basis functions are obtained by a knot vector, which defines the functions' break points, in the form as below [11]:

$$\{\underbrace{0, \dots, 0}_{p+1}, u_{p+1}, \dots, u_{m-p+1}, \underbrace{1, \dots, 1}_{p+1}\} \quad (3)$$

One advantage to use NURBS is that a second-degree NURBS curve is accurate enough to represent arc, which is a common form of leading and trailing edges, while other forms of curves such as Bezier curves would fail in representing arcs. Therefore, a 2D blade profile can be represented by two composite NURBS curves: a pressure side curve and a suction side curve, with each composite curve consisting of three NURBS curves. Take the pressure side curve as an illustration: first using second-degree NURBS curves to represent the leading edge arc and trailing edge arc respectively; then using a third-degree NURBS curve to represent the main body of the pressure side curve; finally merging these three NURBS curves into one composite NURBS curve. This method guarantees C1 continuity at the points of conjunction. Figure 2 gives an example of rotor blade hub profile represented by NURBS.

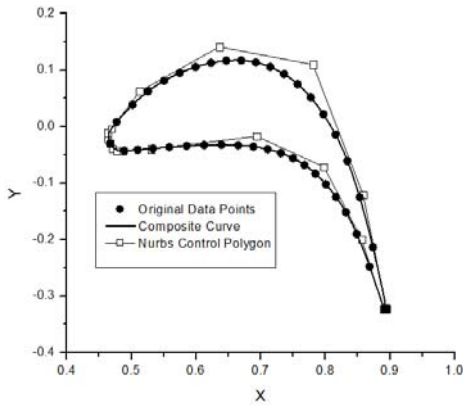


Fig. 2 Rotor blade hub profile represented by NURBS

A blade stacking line is represented by a third degree NURBS curve with seven control points. Optimization programs are used to modify the positions of NURBS control points excluding their corresponding weights.

NURBS skinning technology [11] is used to interpolate sections between given blade profiles along the blade height and define a 3D blade surface geometry. In this paper, a blade stacking line and several two-dimensional slices of control sections as described above at blade hub, tip and some other span positions along the blade height are first given, then a three-dimensional blade surface is constructed by the NURBS skinning technology. By modifying the NURBS blade stacking line, the skinned blade surface can be modified accordingly. Therefore, according to different blade optimization design objectives, the three-dimensional blade deformation can be easily achieved. Figure 3 gives an example of a leaned rotor blade and shows the way to make a leaned blade by the above techniques with the analytically represented control sections and the lean stacking line used to add circumferential displacement.

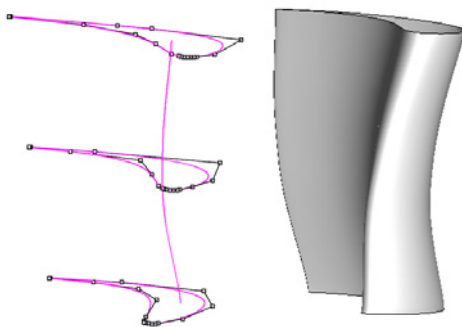


Fig. 3 Leaned rotor blade made by NURBS techniques

Non-axis-symmetric End-wall Representation

The end-wall representation represents the end-wall surface in one blade passage. By adding a radial coordinate change ΔR to an axis-symmetric end-wall, the non-axis-symmetric end-wall can be achieved. Periodical boundaries and meridian curves are used to define the boundaries of an axis-symmetric end-wall.

The radial coordinate change function $\Delta R(s, t)$ is a NURBS surface [11] defined in parametric space $(\Delta R, s, t)$. The NURBS surface is defined as follows:

$$S(u, v) = \frac{\sum_{i=0}^n \sum_{j=0}^m N_{i,p}(u)N_{j,q}(v)w_{i,j}P_{i,j}}{\sum_{i=0}^n \sum_{j=0}^m N_{i,p}(u)N_{j,q}(v)w_{i,j}} \quad (4)$$

Where $(n+1) \times (m+1)$ control points $P_{i,j}$ construct the control net of the surface, with three coordinates $\Delta R, s$ and t . $w_{i,j}$ are weights. p and q are degrees of the NURBS surface. B-Spline basis functions $N_{i,p}(u), N_{j,q}(v)$ are defined on knots $\{u_0, u_1, \dots, u_{n+p+1}\}$ and $\{v_0, v_1, \dots, v_{m+q+1}\}$ respectively. The surface shape can be modified and controlled easily by changing the coordinates of the control points [11].

Figure 4 shows the control point net. The s - and t -coordinates correspond to the dimensionless axial and circumferential location respectively and ΔR is radial coordinate change. The NURBS end-wall surface is made up by three sub-surfaces: the upstream sub-surface, the main sub-surface and the downstream sub-surface to obtain high design freedom. These three sub-surfaces are connected at the leading edge and trailing edge of the blade. The NURBS sub-surfaces have the same degree and the same control point number n in the circumferential direction while in the axial direction, the control point numbers are set to K_u, K_p, K_d respectively. By changing the parameter ΔR to non-zero, the original smooth end-wall surface then becomes non-axis-symmetric.

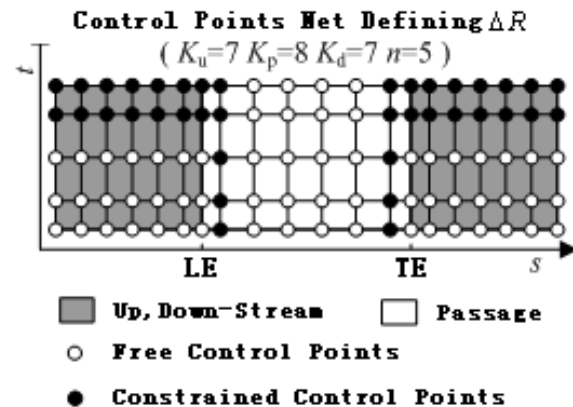


Fig. 4 NURBS control point net of the radial coordinate change function

Optimization Strategy

The purpose of the optimization strategy is to assist turbine designers to coordinate their knowledge of aerodynamics with modern optimization technologies, to expand design exploration scopes and to accelerate design processes of high efficiency steam turbine stages with stator and rotor blades. A computer aided optimization package software has been used as an optimization platform in the current optimization system. Several typical optimization methods are applied in this developed system.

First, design of experiment (DOE) can be used in pre-process to explore the high-dimensional design space and to determine the most influential variables so that the number of design variables can be reduced.

Second, during the optimization process, global optimization algorithms such as genetic algorithms (GA) and adaptive simulated annealing algorithm (ASA) can be applied to estimate the potential

global optimal result.

Finally, at the end of the optimization process, approximation algorithms such as response surface model (RSM) can construct approximation by fitting the data obtained from the DOE and GA study.

For turbine stage optimization, DOE can be used at first to assess the influence of parameters to the optimization objectives; ASA can be applied in single objective optimization problems and Non-dominated Sorting Genetic Algorithm II (NSGAI) can be applied in multi-objective optimization problems.

INFLUENCE OF SEAL LEAKAGE

To better optimize the design problem considering seal leakage, a general view of the flow patterns with leakage should first be derived and the influence of leakage to the main flow should be investigated.

The study has been carried out on a two-stage typical high-pressure turbine stage for 1000MW-class large-scale super-critical pressure steam turbines. The configuration of the turbine stage is demonstrated in Figure 5.

All the blades are shrouded with labyrinth seals on hub and tip. The first stage inlet total and the second stage outlet static pressures are 20.53MPa and 16.40MPa. The design inlet total temperature is 835K, the design mass flow rate is 790.59 kg/s and the rotor rotational speed is 3600rpm. The power output of the two stages is around 60MW. Table 1 gives the key geometrical design parameters of the stator and the rotor blades. These design parameters were extracted from actual turbine configurations and were specially prepared for the current leakage study and the optimization design study. Therefore, the results of this study can be used in actual design practice.

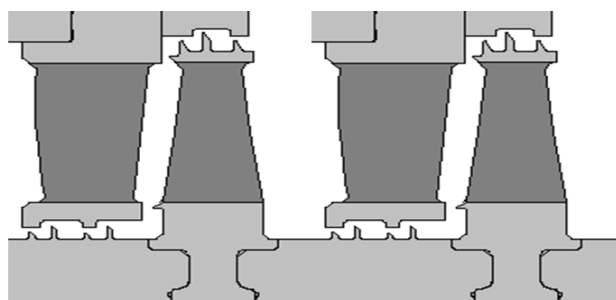


Fig. 5 Turbine stage configuration overview

Table. 1 Key geometrical design parameters for the two stages

Parameter	Stator	Rotor
Hub radius(m)	0.4575	0.4575
Tip radius(m)	0.5325	0.5325
Blade number	42	70

The study of the leakage influences and inter-stage reciprocal interactions involves two CFD calculations. One was to calculate the main flow of the stage without considering the leakage flows, the other was to calculate the main flow and all leakage flows through the labyrinth seal paths. Both calculations were carried out in the same original turbine stages. Real gas effect was also considered in the calculation. The grid node number of the meshes of only the main flow is 1304919 and the calculation meshes with the seal paths are shown in Figure 6, where the grid node number of the meshes is 2885560.

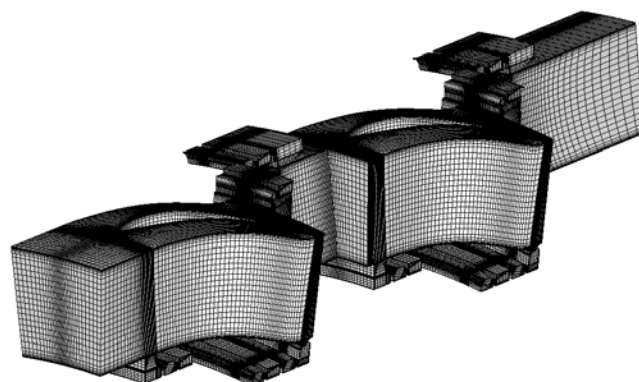


Fig. 6 Calculation meshes with seal paths

By comparing these CFD calculation results, the influence of leakage flows can be determined. Table 2 compares the aerodynamic parameters of the calculation result. From this comparison, we can see that leakage has a negative influence to the flow, which reduces the efficiency of the stage and increases the mass flow rate of the stage inlet.

Table. 2 Global parameters comparison

	without leakage	with leakage
fluid model	real gas	real gas
2 stage total-static efficiency(%)	95.35	93.57↓
mass flow(kg/s)	796.28	816.89↑

Figure 7 compares the entropy increase of the meridional view of these two calculations. On average, the entropy in the calculation with leakage is much higher than that without leakage. When the fluid of the main flow goes through the seal path, its entropy increases sharply in the seal paths and when these leakage flows return to the main flow, their high entropy increase, which indicates high loss, joins the main flow, making the energy of the main flow reduce and the loss of the main flow increase. The entropy increase is most obvious at the positions near hub and tip, where the leakages flow out and into the main flow. As for inter-stage reciprocal interactions, the influence of leakage still lasts downstream and gradually moves from the end walls to the middle of the blades.

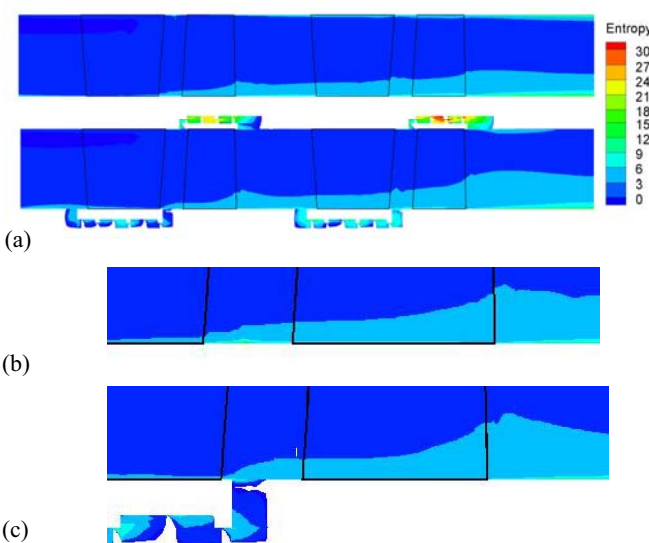


Fig. 7 Meridional view of entropy contours without leakage (top of a), with leakage (bottom of a), close-up of first stage hub without leakage (b) and close-up of first stage hub with leakage (c)

In order to understand how the losses move from the end-walls to the middle of the blade channel, seven monitoring sections along the turbine stages have been chosen. Figure 8 shows the seven monitoring sections along the turbine stages and Figures 9 show entropy contours on these seven sections. Figure 9(a) shows the entropy distribution on the section (a), which is located just upstream of the nozzle hub leakage. The suction of flow through the leakage gap increases the entropy near the hub, bringing in loss to end wall boundary layer. Figure 9(b) shows the entropy distribution at section (b), which is a section across the first nozzle. The entropy at the hub of the suction side suggests the formation of horseshoe vortex. Figure 9(c) to (g) show the entropy distributions of the sections along the flow to the correspond positions. All contours have two characteristics. At hub, it shows the trend of the leakage effects moving from the end wall towards the middle of the blade channel. At tip, it shows the reduction of loss caused by leakage flow at blade tip, which takes the tip end wall boundary layer away to the seals and compensates the mass flow increase by the re-injection of leakage flow at hub.

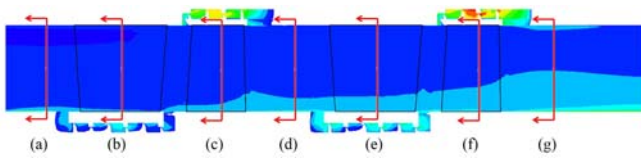


Fig. 8 Monitoring sections along the turbine stages

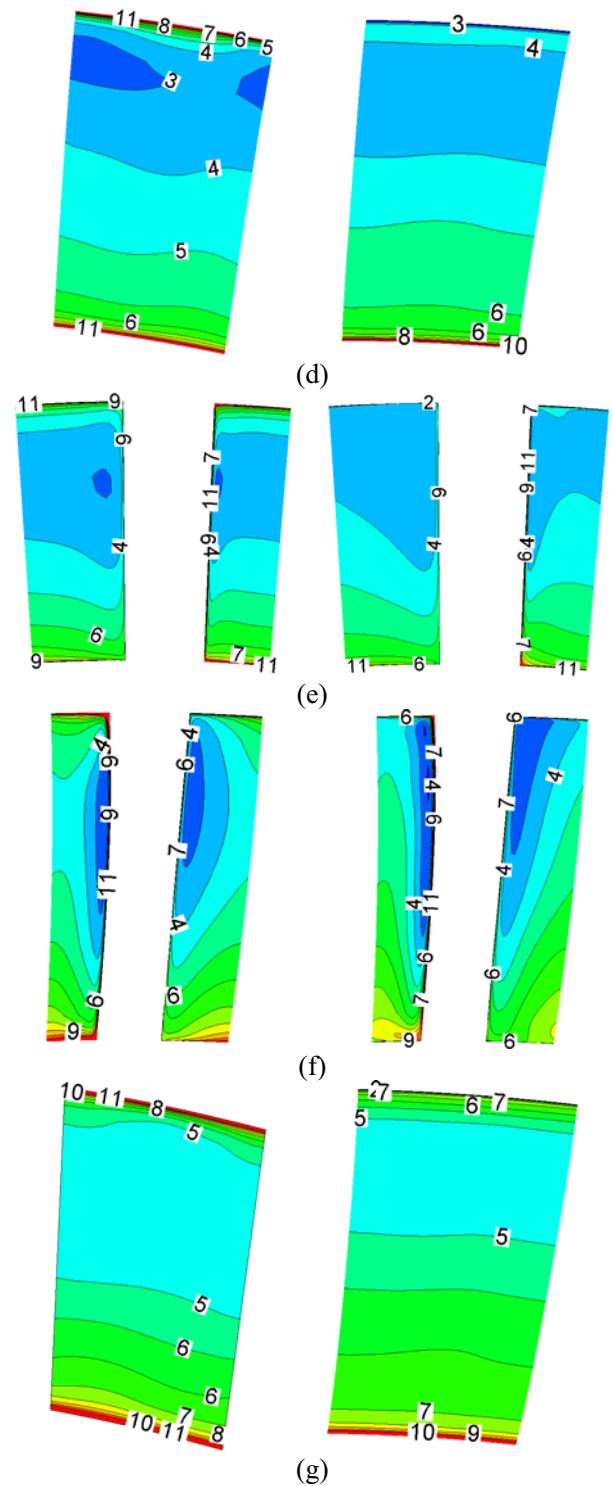
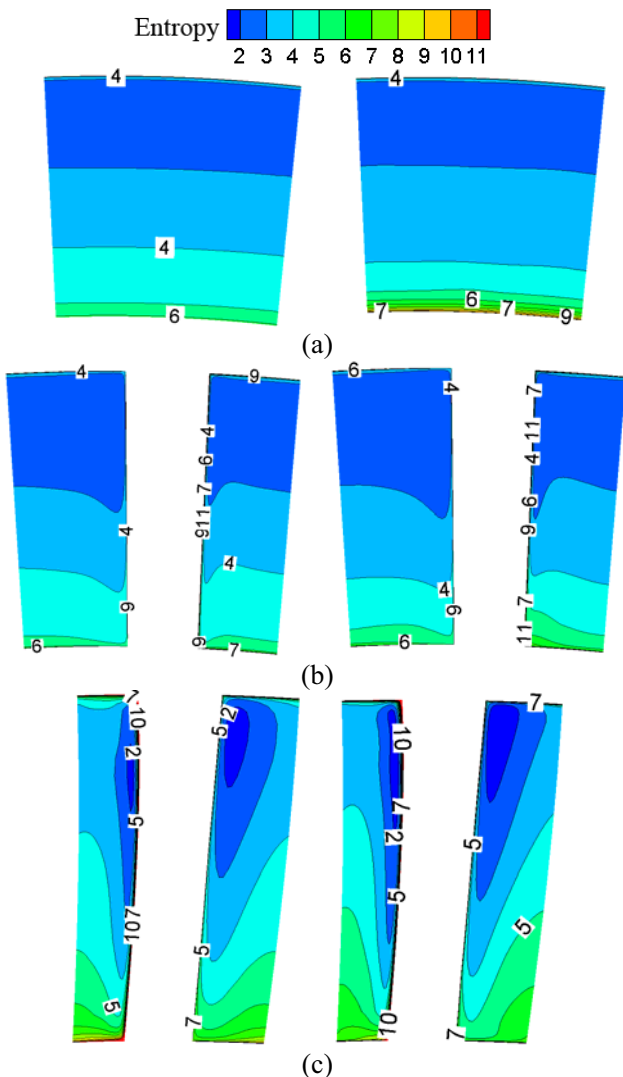


Fig. 9 Entropy contours on seven sections along the turbine stages (left: without leakage, right: with leakage)

As we observe the entropy distributions carefully, the influence of leakage can be summarized in four aspects. (1) Leakage affects both upstream and downstream of the flow. As the flow goes downstream, the effects move from the end wall towards the middle of the blade channel. (2) The loss mechanism of leakage to the main flow may be in two ways. One is when the leakage re-joins the main flow, it brings in the low energy fluid and mixes them with the main flow, which reduces the energy of the main flow and produces a disturbance. The other one is that leakage increases the pressure gradient between the pressure side and the suction side, thus aggravates the secondary flow near the suction side. (3) The influence

of leakage can add on as the flow goes downstream so that the impact can either expand greatly, making the main flow increasingly worse. However these leakage impacts may be compensated with each other if the position and mass flow would be designed carefully. (4) Geometry is also an important factor. For the positions where the leakage flows into the seal, the seal gap should be narrowed to reduce the leakage mass flows. For the positions where the leakage joins the main flow, wide seal gap may reduce the effect of the leakage to the main flow.

Understanding the influence of the leakage flows and the inter-stage reciprocal interactions can assist the optimization process. Using validated calculation method, optimization can take the influence of leakage into consideration and explore an optimal result which reduces the negative effects of leakage and inter-stage reciprocal interactions.

STEAM TURBINE STAGE OPTIMIZATION

Instead of optimization of one turbine stage in the previous study, successive two stages in a typical high-pressure steam turbine as described above is chosen for the present fluid dynamic optimization design study. The boundary conditions are the same as above. Hub and shroud leakage has been considered in the optimization. Only the rotor blades of the first and the second stages are optimized in the present study.

The turbine stage mesh configuration is shown in Figure 10, whose grid node number is 752003. By creating a proper template file and using batch processing, a two stage grid can be generated automatically.

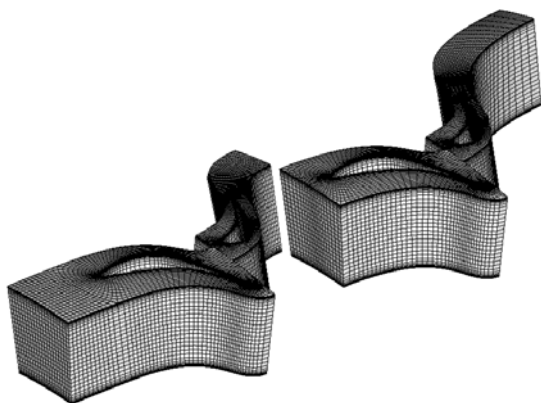


Fig. 10 CFD mesh of the turbine stages

In the CFD evaluation, a simpler model of hub and shroud leakage using sources and sinks on the end-wall meshes was employed to reduce CPU time of each calculation since the full labyrinth seal path model takes too much time and resources. This simple model was validated to be able to simulate the characteristics of the leakages. Table 3 shows the global parameters of the simple model and the seal path model, in which both calculations were carried out on fine meshes. In the comparison, the errors of the global parameters are small. Figure 11 shows the velocity vectors of leakage flows through blade tip end wall with static pressure colour contours. We can see leaving and re-entering leakage flows just upstream and downstream of rotors. Figure 12 compares the entropy distributions of the flow path. The simple model has nearly the same pattern as the seal path model.

Table. 3 Global parameters validation

	simple model	seal path model	Δ
fluid model	ideal gas	real gas	-
2 stage total-static efficiency(%)	93.14	93.57	-0.43
mass flow(kg/s)	802.81	816.89	-1.7%

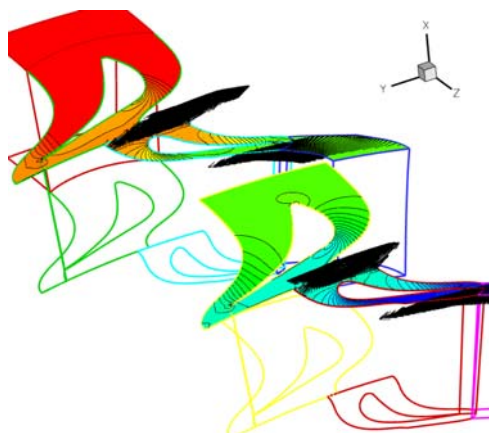


Fig. 11 Velocity vectors of leakage flows through blade tip end wall

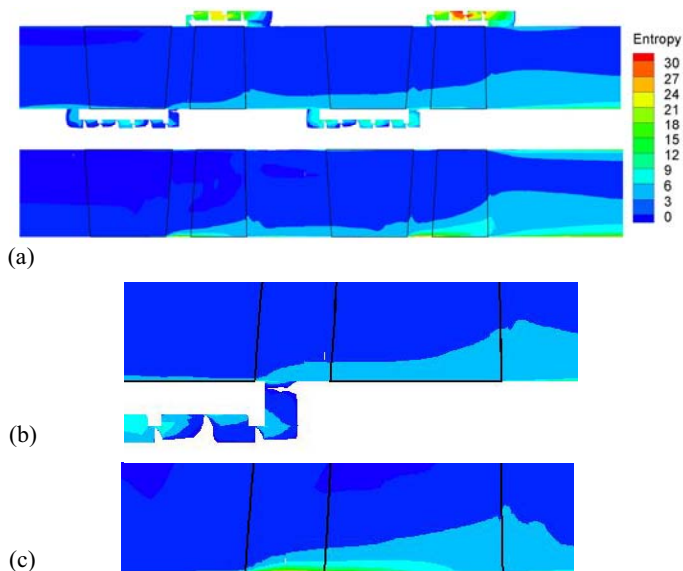


Fig. 12 Meridional view of entropy contours with full mesh leakage calculation (top of a), with simple leakage calculation (bottom of a), close-up of first stage hub with full mesh leakage calculation (b) and close-up of first stage hub with simple leakage calculation (c)

The optimization process was divided into two parts. The first part was to use Design of Experiment (DOE) to explore the high-dimensional design space and determine the most influential design variables. The second part was to apply global optimization algorithms to the optimization problem to estimate the potential global optimum result.

Twist stacking line optimization was implemented to the rotor blades design optimization process. As we introduced two-objective optimization method to maintain the main mass flow rate as a constant design value, the multi-objective optimization strategy NSGA II (Non-dominated Sorting Genetic Algorithm) was used in the second part of the optimization. One objective function was the maximum total enthalpy efficiency with the leaving energy considered as a loss. The efficiency was calculated using the CFD

results, which was defined as follows,

$$\eta = \frac{\text{power of two stages}}{\dot{m} \cdot (h_{0T} - h_{2s})} \quad (5)$$

The other objective function was the minimum mass flow rate difference from the design mass flow rate. The number of design variables was 14 for the optimum design of twist of the both rotor stacking lines.

Part One: DOE studies

The purpose of DOE studies is to analyze the influence of design variables and their changes to the objective function and the constraints. In this optimization, the Latin hypercube technique is applied since it has the advantage to get much information with respectively little time. The magnitude and tendency of the variables' influence is shown in Figure 13. The length of the bars indicates how much a variable affects the objectives and the color indicates the direction of the influence, where red means positive correlation with the total enthalpy efficiency, and blue means negative correlation.

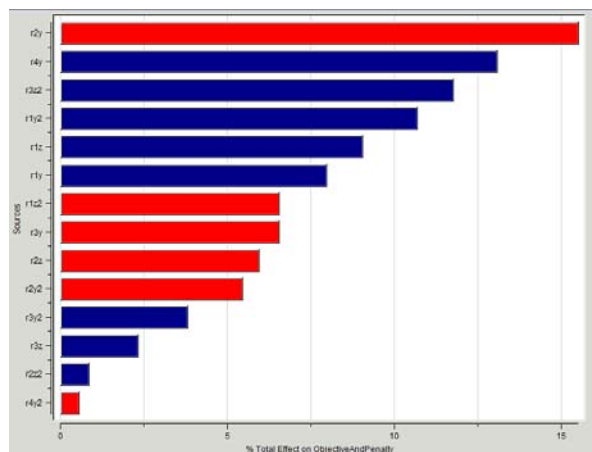


Fig. 13 Pareto graph of the DOE results

Using Figure 13, influential factors can be determined. Top four parameters in Figure 13 are with the influential rates above 10%. By interpreting the results of Figure 13, the tendency of the change to potential optimum blade shape stacking line can be estimated as Figure 14. The first rotor blade tends to twist to the pressure side near tip. The second rotor blade tends to twist to the suction side at the hub.

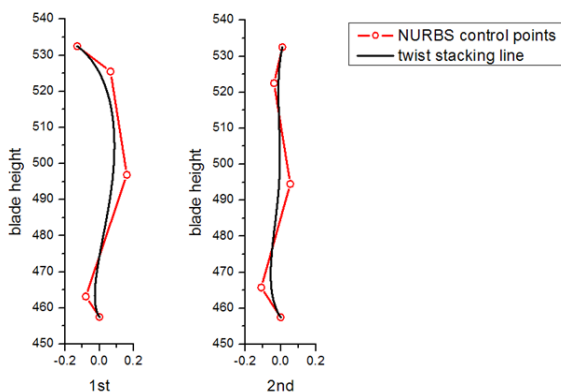


Fig. 14 Tendency of the optimum blade stacking line change of the first and the second stage rotor blades

Part Two: global optimum result by NSGA-II

The optimization history is shown in Figure 15. As the original point is indicated in Figure 15, we can see that the efficiencies of most exploration results are above the original efficiency, which shows the effectiveness of the optimization strategy.

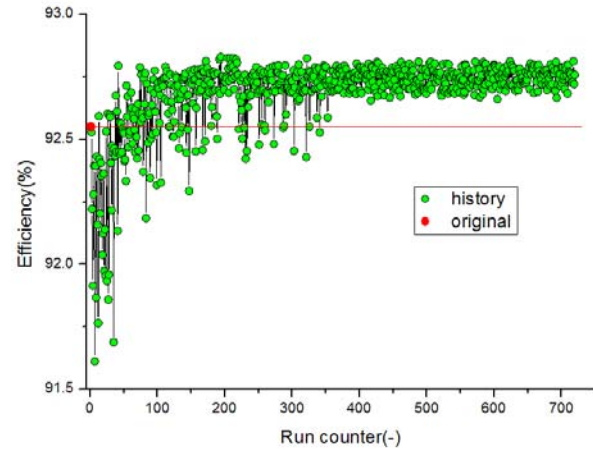


Fig. 15 Efficiency optimization history

For multi-objective optimization problems, the selection of its optimal solution is different from the single objective problem. In single objective problems, the maximum or minimum value of the solution is viewed as the optimal solution. In multi-objective problems, since different objective functions may conflict with each other, it is difficult to find an optimal solution to achieve the best situation of all objective functions. Therefore, a solution set is viewed as the optimal result for multi-objective optimization problems. Solutions in the optimal solution set are equal, since one objective function cannot be improved without weakening at least one other objective function. The optimal solution set is called non-dominated solutions or Pareto optimal solutions. By plotting all feasible solutions in a n-dimensional space, where n equals the number of objective functions, the boundary of the space occupied by these solutions is then the Pareto optimal solution, which is also called the Pareto front. Figure 16 shows the Pareto front of the optimization. The optimal solution for this optimization is selected on the Pareto front within the mass flow constraints as $\pm 0.5\%$. The original and optimal points are also indicated in Figure 16. The original efficiency of the stage is 92.55%. After the global exploration by NSGA-II, the largest improvement of the stage efficiency within the mass flow limitation was **0.21%** with the mass flow rate reduced by **0.46%**. The optimal result with least mass flow difference has increased the efficiency of the stage by **0.17%** and only reduced the mass flow by **0.01%**.

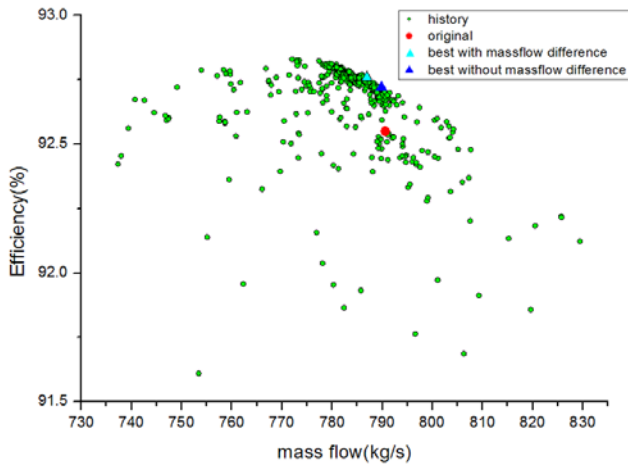


Fig. 16 Pareto frontier of the optimization

Figure 17 compares the original and the optimal blades of the first and the second rotor blades. Figure 18 compares the control sections and the blade trailing edges of the original and optimal blades. The optimal blades have slight twists in comparison with the original blades. The first rotor blade twisted towards the pressure side at blade tip while the second rotor twisted to the pressure side at tip and to the suction side at hub. The optimal results corresponded with the tendency of DOE analysis to some extent.

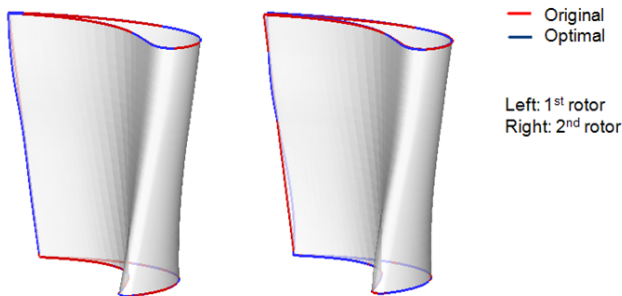


Fig. 17 The original and The optimal blades

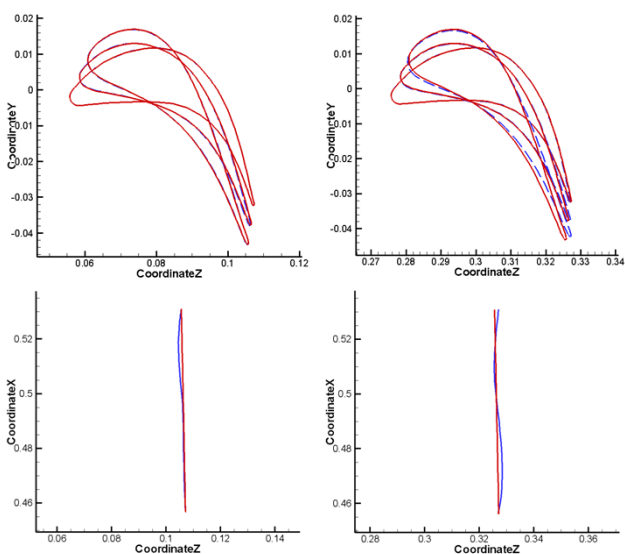


Fig. 18 Blade control sections and trailing edges (left: 1st rotor, right: second rotor; red: original, blue: optimal)

Figure 19 compares the mass-flow distributions of the original and optimal blades. For the optimal blades, more uniform mass flow distributions are achieved and there is more mass flow pass through blade hubs and less mass flow pass through blade tips while in the original blades, mass flow tends to pass through the upper part of the blade, which is not the main part to produce power, thus makes loss in utilizing the flow energies.

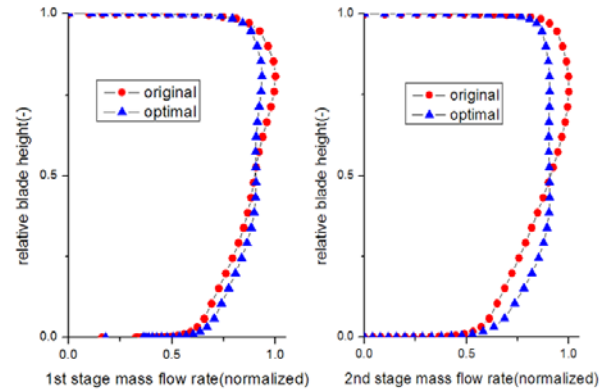


Fig. 19 Mass-flow distributions (left: 1st rotor, right: second rotor; red: original, blue: optimal)

Figure 20 compares the entropy contours near the stage outlet of the original and optimal blades. The entropy of the optimal stage is lower than the original blade on average, especially at the position near the tip end wall and the hub.

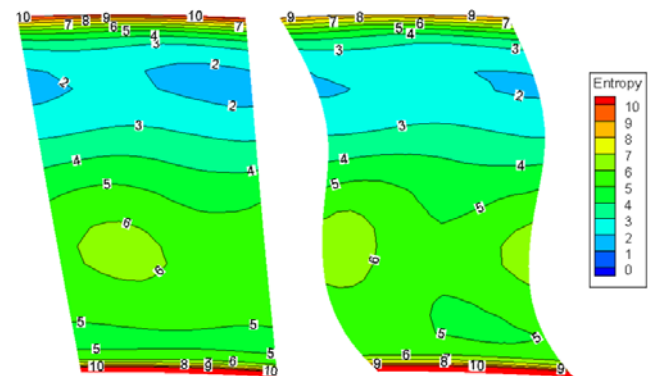


Fig. 20 Stage outlet entropy contours (left: original, right: optimal)

CONCLUSIONS

An advanced and more applicative study to enhance the current optimization methodology from a single turbine stage to two turbine stages with stator blade hub leakage and rotor blade tip leakage influences is presented in this paper.

The leakage influences and inter-stage reciprocal interferences have been investigated. Analysis shows that: the existence of leakage has a negative influence to the flow, which reduces the efficiency of the stage and increases the mass flow rate of the stage inlet. The main effects of leakage can be summarized in four aspects: (1) Leakage affects both upstream and downstream of the main flow and move from the end wall towards the middle of the blade channel as the flow goes downstream. (2) The loss mechanism of leakage to the main flow may be the mixture of the low

energy leakage flow with the main flow and the aggravation of secondary flow in the suction side. (3) The influence of leakage can add on as the flow goes downstream. (4) Geometry is also an important factor.

For the validation and demonstration of this improvement for the current optimum design system, both rotors of a two-stage high-pressure turbine stage in a typical large scale steam turbine are designed and optimized by the improvement of 0.21%. Considering that only rotor blades of the first and the second stages are optimized and the original efficiency of the stage is already appropriate level for practical designs, the improvement seems to be reasonable and promising.

Design cycle could be greatly shortened by parallel optimization algorithm and cluster PC. Especially seven days could be sufficient for an optimization with one thousand iterations on a 20 CPUs of 2.0G cluster PC.

ACKNOWLEDGEMENTS

This study is supported by Tsinghua-Toshiba Energy & Environment Research Center, the National Natural Science Foundation of China (Grant No. 50676043) and the Special Funds for Major State Basic Research Projects (Grant No. 2007CB210108).

REFERENCES

- [1] Yuan, X., Tanuma, T. et al., 2010, "A CFD Approach to Fluid Dynamic Optimum Design of Steam Turbine Stages with Stator and Rotor Blades" *Proceedings of ASME Turbo Expo 2010: Power for Land, Sea and Air*, ASME paper No. GT2010-22477.
- [2] Wallis, A., Denton, M. et al., 2001, "The Control of Shroud Leakage Flows to Reduce Aerodynamic Losses in a Low Aspect Ratio Shrouded Axial Flow Turbine", *Journal of Turbomachinery*, 123, 334.
- [3] Porreca, L., Behr, T. et al., 2005, "Fluid Dynamics and Performance of Partially and Fully Shrouded Axial Turbines", *ASME Journal of Turbomachinery*, 127, 668.
- [4] Budimir Rosic, John D. Denton, and Graham Pullan, 2006, "The Importance of Shroud Leakage Modeling in Multistage Turbine Flow Calculations", *ASME Journal of Turbomachinery*, 128, 699.
- [5] A. Pfau, A. I. Kalfas, and R. S. Abhari, 2007, "Making Use of Labyrinth Interaction Flow", *ASME Journal of Turbomachinery*, 129, 164.
- [6] Budimir Rosic, John D. Denton, and Eric M. Curtis, 2008, "The Influence of Shroud and Cavity Geometry on Turbine Performance An Experimental and Computational Study—Part I: Shroud Geometry", *ASME Journal of Turbomachinery*, 130, 041001.
- [7] Yuan, X., and Daiguji, H., 2001, "A Specially Combined Lower-Upper Factored Implicit Scheme for Three-Dimensional Compressible Navier–Stokes Equations," *Comput. Fluids*, 30(3), pp. 339–363.
- [8] Yuan, X., Lin, Z. and Tanuma, T., 2003, "Development of High-Order Accurate Computational Fluid Dynamic Method for Steam Turbines," Invited Lecture, Proceedings of 14th International Conference on the Properties of Water and Steam, Organized by IAPWS and Japan Society for the Promotion of Science, Kyoto, Japan, pp. 649-654.
- [9] Yuan, X., Lin, Z., Tanuma, T., Kawasaki, S., Tominaga J. and Lai, Y., 2003, "Applications of Higher-Order Accurate Computational Fluid Dynamic Method to Steam Turbine Blade Designs", Proceedings of International Conference on Power Engineering, 2, pp. 205-210.
- [10] Chen, B., and Yuan, X., 2009, "Advanced Aerodynamic Optimization System for Turbomachinery", *ASME Journal of Turbomachinery*, 130, 021005.
- [11] Piegl, L. and Tiller, W., 1997, *The NURBS Book*, Springer, New York.